Sarah Grube*, Maximilian Neidhardt, Sarah Latus, and Alexander Schlaefer

Influence of the Field of View on Shear Wave Velocity Estimation

https://doi.org/10.1515/cdbme-2022-0011

Abstract: Tissue elasticity contains important information for physicians in diagnosis and treatment, and, e.g., can help in tumor detection because tumors are stiffer than healthy tissue. Ultrasound shear wave elastography imaging (US-SWEI) can be used to estimate tissue stiffness by measuring the velocity of induced shear waves. Commonly, a linear US probe is used to track shear waves at a high imaging frequency in 2D. Real-time US-SWEI is limited by the required time for data processing. Hence, reducing the imaging field of view (FOV) is beneficial as it decreases the size of the acquired data and thereby the acquisition, transfer and processing time. However, a decrease in the FOV has the disadvantage that shear waves are tracked over a smaller distance and thus, also fewer sampling points are available for velocity estimation. This trade-off between a smaller FOV and thus, a smaller data size, and the accuracy of shear wave velocity estimation is investigated in this work. For this purpose, shear waves were tracked with a linear US probe in gelatin phantoms with four different stiffness values. During data processing, we reduced the FOV virtually from $38.1\,\mathrm{mm}$ to $2.1\,\mathrm{mm}$. It was found that a reduction of the FOV to $4.5\,\mathrm{mm}$ leads to an overestimation of up to five times larger shear wave velocities but still allows to distinguish between phantoms of different stiffness. However, not all estimated velocity values could be clearly assigned to the correct stiffness value. The smallest studied FOV of $2.1\,\mathrm{mm}$ was not sufficient for distinguishing between the phantoms anymore.

Keywords: Ultrasound, Shear Wave Elastography, Field of View, Number of Elements, High-frequency US imaging.

1 Problem

Mechanical properties of tissue can help indicate diseases and assist physicians in diagnosis and treatment. Tumors, e.g., can be distinguished from healthy tissue by their mechanical properties because they are stiffer [3]. Shear wave elastography imaging (US-SWEI) can be used to estimate tissue stiffness and is already applied in clinical practice in, e.g., staging liver fibroses [7]. The principle of US-SWEI is to induce a shear wave in the tissue. The shear wave propagation velocity depends on tissue stiffness and can be directly connected to the Young's modulus [2]. Hence, US-SWEI allows to estimate quantitative stiffness values from tissue. Often high frequency 2D US-SWEI with a linear probe is performed. To estimate the shear wave velocity, the shear wave propagation is tracked over time with US. As in soft tissue shear waves travel at a velocity of $2\,\mathrm{to}\,10\,\mathrm{m/s}$ [5], a high imaging frequency of about $1000\,\mathrm{Hz}$ is required to fulfill the Nyquist theorem. Hence, for real-time shear wave velocity estimation, it is important to acquire and process US images with at least $1000\,\mathrm{Hz}$. In Engel et al. [4] the required processing time was reduced by using an inversion of the first-order wave equation for shear wave velocity estimation. A near-real-time shear wave velocity estimation was possible within four seconds. However, additional methods can be used to further decrease the processing time. In this work the possibility to enable a faster acquisition and processing time by reducing the data size is investigated. For this purpose, the field of view (FOV) size is decreased by decreasing the number of piezo elements used for data acquisition. By decreasing the number of piezo elements but keeping their pitch constant, the same lateral resolution can be reached with the drawback that the shear wave is tracked with a smaller FOV. In this work we investigate this drawback and thus, the influence of lateral FOV size on shear wave velocity estimation. Therefore, shear waves were tracked in soft tissue phantoms of different stiffness. The FOV size was reduced in five steps from $38.1\,\mathrm{mm}$ to $2.1\,\mathrm{mm}$. The influence of the FOV size on shear wave tracking was evaluated based on the ability to distinguish between different phantom stiffness and the reproducibility of shear wave velocity estimations compared to the largest FOV studied in this work.

2 Material and Methods

The methods used to investigate the influence of the FOV on shear wave velocity estimation are described in the following. First, the experimental setup and the parameters for data acquisition are presented. Second, the required steps to reconstruct the US images and estimate shear wave velocities are described.

***Corresponding author: Sarah Grube,** TUHH, Am Schwarzenberg-Campus, Hamburg, Germany, e-mail: sarah.grube@tuhh.de
Maximilian Neidhardt, Sarah Latus, Alexander Schlaefer, TUHH, Hamburg, Germany

2.1 Experimental Setup

The setup is composed of a linear piezo-actuator with an attached needle to induce shear waves and a linear US probe for US-SWEI. A schematic of the experimental setup is shown in Figure 1 and the final setup can be seen in Figure 2. The needle was inserted by a UR5 robot (Universal Robots, DK) with an angle of 20° to a depth of $30\,\mathrm{mm}$ into the gelatin phantom to enable a large contact area between needle and phantom. The piezo-actuator (PSt 150/7/140 VS12, Piezomechanik GmbH, DE) excites a continuous sinusoidal vibration of the needle in insertion direction. Due to the needle vibration, shear waves are generated that propagate through the phantom perpendicular to the insertion direction. The vibration frequency was set to $300\,\mathrm{Hz}$. The used linear US probe (Ultrasonix *L14-5\38*) has 128 elements and a pitch of $0.3\,\mathrm{mm}$, resulting in a maximum FOV of $38.1\,\mathrm{mm}$. Shear waves were tracked over time with plane wave imaging and an imaging frequency of $6000\,\mathrm{Hz}$. For each acquisition, 70 US images at a depth between $0.1\,\mathrm{m}$ and $0.3\,\mathrm{m}$ were acquired with a 256 channel US system (Griffin, Cephasonics, USA) in SUPRA [8]. The probe was mounted to a UR3 robot (Universal Robots, DK) and was aligned parallel to the shear wave propagation direction. The UR3 and UR5 robots were spatially calibrated to each other to automatically position the shear wave stimulator and linear US probe, while keeping the relative position between the US probe and the shear wave stimulator constant.

Phantoms of four different gelatin concentrations ($7.5\,\%$, $10\,\%$, $12.5\,\%$, $15\,\%$) were produced with $1\,\mathrm{g}$ graphite scatterer per $100\,\mathrm{ml}$ water. The gelatin concentrations were chosen, such that stiffness values correspond to soft tissue [6]. In each of the four phantoms, the needle was inserted at 18 different positions to increase the scatterer variability. For each position, 10 acquisitions were done to be able to evaluate the repeatability. This whole acquisition procedure was repeated three times, each time a different side of the phantoms was used to get more variation in scatterer distribution but still ensure the same phantom stiffness.

2.2 Data Processing

After image acquisition, the raw plane wave US data were first processed to reconstruct the US images. Afterwards, the US images were processed in further steps. The Loupas' autocorrelation algorithm [1] was used to estimate the shear wave position based on scatterer motion in the spatio-temporal US images. Noise in the US images was reduced by a median filter and morphological operations. A space-time map was generated to estimate the shear wave velocity. The spatio-temporal US images (2D+t) were cropped to an imaging depth of $7.5\,\mathrm{to}$

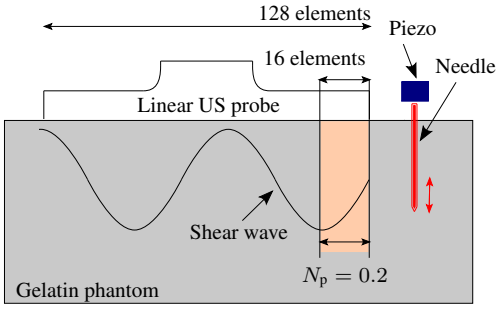

Fig. 1: Schematic of the experimental setup with a needle attached to a linear piezo-actuator for shear wave excitation and a linear US probe for shear wave tracking. The virtually reduced lateral FOV sizes are shown exemplarily for $38.1\,\mathrm{mm}$ (128 elements) and $4.5\,\mathrm{mm}$ (16 elements). N_p describes how many shear wave periods are visible in the FOV.

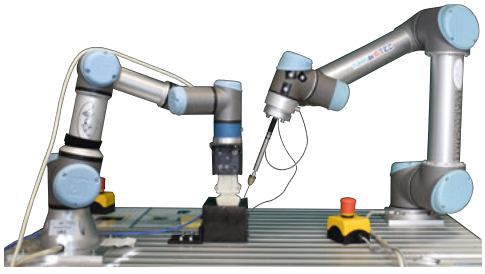

Fig. 2: Experimental setup to generate and track shear waves. Two robots are used to automatically position needle and linear US probe with a fixed orientation relative to each other.

$12\,\mathrm{mm}$ and averaged along the axial axis. This space-time map represents the shear wave motion along the lateral axis (Figure 3a) and was transferred into the frequency domain by a Fast Fourier Transformation (Figure 3b). The maximum intensity value in Figure 3b around $300\,\mathrm{Hz}$ represents the shear wave properties and allows to estimate the shear wave frequency f_sw and wavenumber $\tilde{\nu}_\mathrm{sw}$. Accordingly, the shear wave velocity can be estimated by the position of the maximum with

$$c_\mathrm{sw} = \frac{f_\mathrm{sw}}{\tilde{\nu}_\mathrm{sw}}. \tag{1}$$

For each phantom concentration, shear wave velocities with a larger deviation from the median velocity than three-times the standard deviation were marked as outliers. A probe with a smaller FOV was simulated by not taking the raw data from all 128 piezo elements for US image reconstruction as it is shown in Figure 1. Note that the element pitch is kept constant. The investigated number of piezo elements N_elem for image reconstruction with the resulting FOV are shown in Tabular 1. Furthermore, it is listed, how many periods N_p of the continuously excited shear waves are visible in that FOV if a $15\,\%$ gelatin phantom is assumed and thus a shear wave velocity of $6.62\,\mathrm{m/s}$ [5]. As exemplarily shown in Figure 1, about 1.74

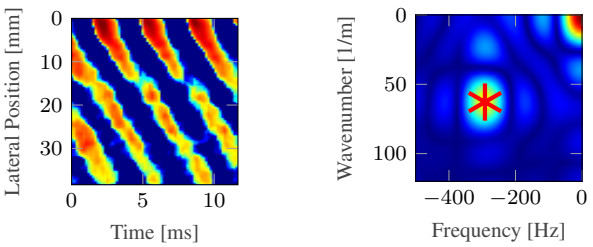

(a) Space-time domain. **(b)** Frequency domain.

Fig. 3: Normalized space-time map from shear waves in the $12.5\,\%$ gelatin phantom in (a) time domain and (b) frequency domain. In (b) the maximum is marked with a red asterisk and represents the shear wave frequency f_{sw} and wavenumber $\tilde{\nu}_{\mathrm{sw}}$.

shear wave periods are visible in the maximum FOV of 128 elements. The influence of the FOV on shear wave tracking was evaluated based on the ability to distinguish between different phantom densities and the reproducibility of shear wave velocity estimations compared to the largest FOV studied in this work. The US images were reconstructed in PYTHON and further processing steps were performed in MATLAB.

Tab. 1: Investigated number of piezo elements N_{elem} with the resulting FOV [mm] and the number of periods N_{p} of a shear wave that can be seen in the corresponding FOV when a shear wave velocity of $6.62\,\mathrm{m/s}$ is assumed. In addition, the estimated median velocity v_{med} [m/s] for each phantom is given as well as the number of outliers N_{o} in percent and the repeatability σ_{R} [m/s].

				Gelatin concentration [%]			
N_{elem}	FOV	N_{p}		15	12.5	10	7.5
128	38.1	1.74	v_{med}	7.08	6.01	4.60	3.63
			N_{o}	0.59	0.20	3.92	33.92
			σ_{R}	0.13	0.10	0.07	0.12
64	18.9	0.86	v_{med}	8.19	6.64	5.52	4.13
			N_{o}	1.18	0.78	1.37	15.49
			σ_{R}	0.45	0.29	0.23	0.12
32	9.3	0.42	v_{med}	9.02	7.08	6.19	5.20
			N_{o}	0.39	0	1.76	5.50
			σ_{R}	0.82	0.57	0.52	0.58
16	4.5	0.20	v_{med}	34.56	29.15	24.12	20.00
			N_{o}	6.67	9.41	7.25	6.28
			σ_{R}	7.35	5.40	4.20	3.56
8	2.1	0.10	v_{med}	93.09	55.07	45.63	37.69
			N_{o}	9.80	18.63	13.73	13.73
			σ_{R}	45.43	17.51	20.84	17.16

3 Results

In Figure 4, the estimated shear wave velocities for each gelatin concentration and studied FOV are visualized in boxplots. It can be seen, that a decreased FOV size leads to an overestimation of the shear wave velocity as well as an increase of the standard deviation and number of outliers. When 16 elements are used, the estimated velocities are on average five times larger, with 8 elements eleven-times larger. With a decrease in the FOV size, the estimated velocity range for a specific gelatin concentration increases, and from FOV sizes of 32 elements downwards, the velocity range partially overlaps. It is remarkable that smaller gelatin concentrations lead to more outliers. As for each position ten acquisitions were made, the repeatability was calculated as the standard deviation of the estimated velocities from those 10 acquisitions. In Tabular 1, the median velocity v_{med}, number of outliers and mean repeatability from each phantom concentration is listed. It is visible, that repeatability gets worse with a decrease in the FOV, but is, especially with a smaller FOV, better in softer phantoms.

4 Discussion and Conclusion

Note that a needle was used to generate shear waves, as the focus lies on image processing and not on shear wave generation. Nevertheless, the results can be transferred to non-invasive shear wave generation methods like ARFI. A vibrating needle was chosen to easily enable a continuous propagation of shear waves throughout the whole FOV. The overestimation of the velocity and increase in standard deviation for a reduced FOV can be explained by the fact that fewer shear wave positions over time are known. Consequently, shear wave velocity estimation gets more error-prone. This also explains why more outliers occur and repeatability becomes worse. Especially in hard phantoms, fewer positions of the shear wave are known because they travel fast through the FOV, which results in fewer temporal sampling points. As an example, for a $15\,\%$ gelatin phantom, a single shear wave period is only visible in half as many images as in the $7.5\,\%$ gelatin phantom. This explains why repeatability is better in softer tissues. The increase in outliers in softer gelatin phantoms can be explained by the fact that the needle sticks in softer tissue less strongly to the tissue, which makes shear wave generation and imaging more difficult. Additionally, sound transmission is worse in soft tissue, which leads to stronger shear wave attenuation over time. As a result, shear waves are not visible anymore when they reach the end of the maximum FOV, leading to errors in velocity estimation. This is also the reason why fewer outliers occur for the $7.5\,\%$ phantom when 32 elements are used than when 128 elements are used. Comparing the interquartile ranges of the boxplots in Figure 4, it can be said that with the FOVs corresponding to 128, 64 and 32 elements, all four gelatin concentrations can be distinguished from each other. When 16 el-

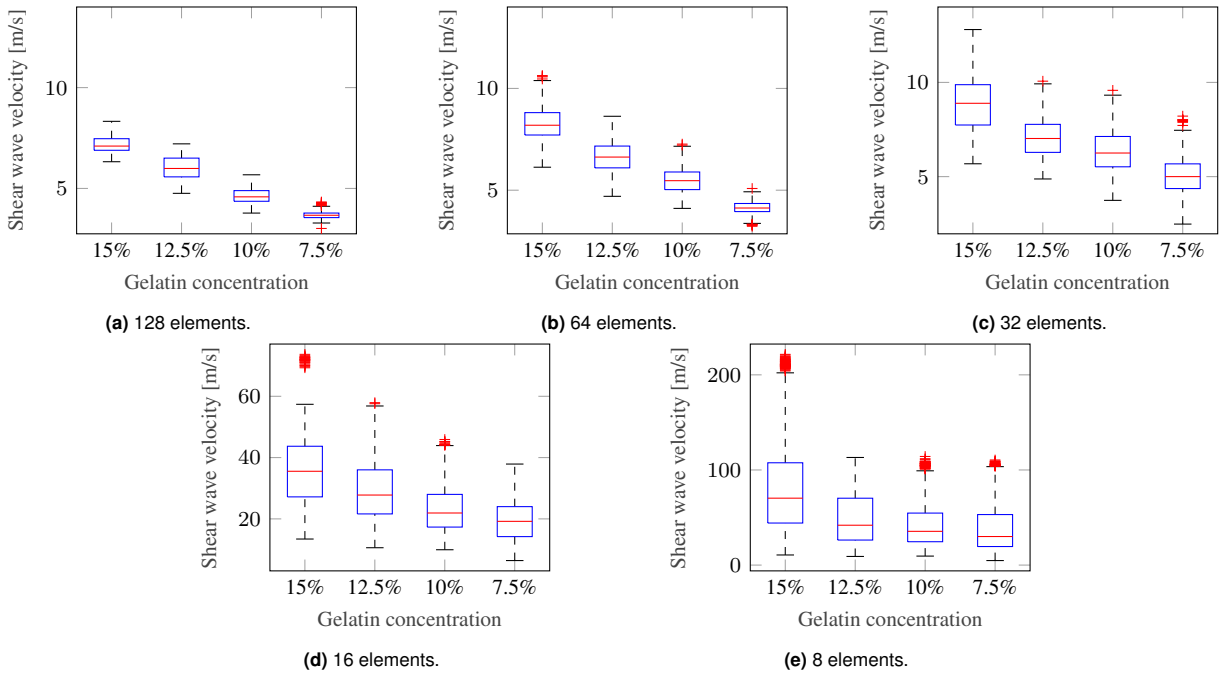

Fig. 4: Boxplots of the estimated shear wave velocities in gelatin phantoms of different stiffness values. The shear wave velocities are estimated when the raw data from 128 (a), 64 (b), 32 (c), 16 (d) and 8 (e) piezo elements are used for US image reconstruction.

ements are used, also a tendency toward higher shear wave velocities in stiffer phantoms occurs. But it is not possible to assign all estimated velocities to the correct concentration. Using only 8 elements in the lateral direction does not allow to distinguish between the different phantoms based on the estimated velocity. In future studies it would be of interest to perform these experiments in real tissue, to demonstrate the transferability of these results to real tissue.

In summary, it can be said that 16 elements are enough to distinguish between tissues with a shear wave velocity difference of at least $1\,\mathrm{m/s}$. It has to be considered that shear wave velocities are highly overestimated. However, this overestimation is consistent over all phantom concentrations. These results are interesting regarding faster data acquisition, transfer, and processing to enable real-time US-SWEI, but also show that probes with only a few elements, such as laparoscopic probes or volumetric probes with 16 x 16 elements, are sufficient to distinguish tissue of different stiffness based on shear wave velocity estimation.

Author Statement

Research funding: This work was partially funded by the TUHH i^3 initiative. Conflict of interest: Authors state no conflict of interest. Informed consent: Informed consent has been obtained from all individuals included in this study. Ethical approval: No ethical approval was necessary for this research.

References

[1] Loupas T, Powers JT and Gill RW. An axial velocity estimator for ultrasound blood flow imaging, based on a full evaluation of the Doppler equation by means of a two-dimensional autocorrelation approach. IEEE UFFC 1995; 42(4):672-688.

[2] Sarvazyan AP, Skovoroda AR, Emelianov SY, Fowlkes JB, Pipe JG, Adler RS et al. Biophysical Bases of Elasticity Imaging. In: Jones JP. Acoustical Imaging, vol. 21. Boston: Springer; 1995223–240.

[3] Chan HW, Uff C, Chakraborty A, Dorward N, Bamber JC. Clinical Application of Shear Wave Elastography for Assisting Brain Tumor Resection. Front Oncol. 2021; 11:619286.

[4] Engel AJ and Bashford GR. Enabling real-time ultrasound imaging of soft tissue mechanical properties by simplification of the shear wave motion equation. International Conference of the IEEE EMBS 2015; 37:3831-3834

[5] Neidhardt M, Ohlsen J, Hoffmann N, Schlaefer A. Parameter Identification for Ultrasound Shear Wave Elastography Simulation. CDBME 2021; 7(1):35-38.

[6] Hoskinsc PR. Principles of ultrasound elastography. Ultrasound 2012; 20(1):8-15.

[7] Ferraioli G, Parekh P, Levitov AB, Filice, C. Shear wave elastography for evaluation of liver fibrosis. JUM 2014; 33(2):197–203.

[8] Göbl R, Navab N, Hennersperger C. SUPRA: Open Source Software Defined Ultrasound Processing for Real-Time Applications. IJCARS 2018; 13:759–767.